Journal of Materials, Processing and Design (2026)
Clausius Scientific Press, Canada

DOI: 10.23977/jmpd.2026.100107
ISSN 2516-0923 Vol. 10 Num. 1

Aqueous Electrolyte Regulation for Enhancing Magnesium–Ion Storage Performance of Spinel–Type $MgFe_xMn_yO_4$ Electrode Materials

Haocai Sun[1,2], Xiaoran Yan[1,2,*], Guang Liu[1,2], Hua Yuan[1,2]

[1] School of Electrical Engineering, Zhejiang University of Water Resources and Electric Power, Hangzhou, Zhejiang, 310018, China
[2] Zhejiang–Belarus Joint Laboratory of Intelligent Equipment and System for Water Conservancy and Hydropower Safety Monitoring, Zhejiang University of Water Resources and Electric Power, Hangzhou, Zhejiang, 310018, China
[*]Correspondence: yanxiaoran1014@163.com

Keywords: Magnesium–ion batteries; $MgFe_xMn_yO_4$; Aqueous electrolyte; Magnesium–ion storage; Cycling stability

Abstract: Spinel–structured magnesium manganate ($MgMn_2O_4$) possesses a three–dimensional tunnel structure that enables fast ion transport and exhibits a relatively high charge–discharge plateau. Therefore, it is a high–performance cathode material with great application potential for magnesium–ion batteries. However, the Jahn–Teller effect induced by high–valence ions such as Mn^{3+} in the material, together with the easy dissolution of Mn^{2+} ions into the electrolyte, severely deteriorates its electrochemical cycling stability and rate capability. To address these issues, in this work, spinel–type $MgFe_xMn_yO_4$ nanomaterials were synthesized via the sol–gel method. Using 0.5 M $MgCl_2$ aqueous solution as the electrolyte, different amounts of manganese acetate were added to effectively inhibit the Jahn–Teller effect and Mn^{2+} dissolution, and the influence of Mn salt concentration in the electrolyte on the electrochemical performance of the electrode material was systematically studied. X–ray diffraction (XRD), scanning electron microscopy (SEM), and nitrogen adsorption/desorption measurements were employed to characterize the phase composition and microstructure of the prepared materials. The results show that the material exhibits optimal electrochemical performance when the concentration of manganese acetate in the electrolyte is 2.45 mM. In this study, the dual regulation of electrode materials and electrolytes effectively improves the magnesium ion storage performance and cycling stability of electrodes, which is of great significance for the development and application of aqueous magnesium–ion batteries.

1. Introduction

In recent years, with the increasing intensification of the energy crisis and growing prominence of environmental issues, the research and development of renewable energy (such as solar and wind power generation) have attracted widespread global attention. However, such energy sources

generally suffer from the inherent defect of intermittent energy supply, so it is necessary to rely on energy storage equipment to realize energy storage and on–demand utilization[1]. Energy storage has thus become a key core means to achieve comprehensive, clean and efficient utilization of energy, and has become a research focus of researchers around the world. In the field of energy storage, chemical power sources occupy a pivotal position. Among them, lithium–ion batteries have achieved widespread commercial application, but with the rapid development of social science, technology and economy, they have gradually been unable to meet people's demand for higher energy density. Moreover, lithium–ion batteries currently using graphite as the negative electrode material have a serious problem of lithium dendrite growth, which greatly affects the safety and cycle life of the batteries[2,3]. In addition, with the large–scale development and consumption of lithium resources, their reserves are becoming increasingly scarce, leading to high production costs; in contrast, magnesium resources on earth are extremely abundant, making metallic magnesium low–cost. Furthermore, magnesium ions carry two units of positive charge and can provide higher energy output. Therefore, the research and development of rechargeable magnesium–ion batteries have gradually become the focus of researchers' attention[4]. To further optimize the environmental friendliness, safety of the magnesium–ion battery system and reduce production costs, the research direction of using aqueous solutions as electrolytes has received widespread attention and in–depth exploration[5]. In summary, aqueous magnesium–ion batteries, with their unique advantages, are expected to become the ideal energy storage device for the next generation.

Since magnesium and lithium metals possess similar chemical properties, and the ionic radii of Mg^{2+} and Li^{+} are 0.43 nm and 0.38 nm, respectively, which are quite close, magnesium–ion batteries can be investigated based on the existing research foundation of lithium–ion batteries[6,7]. Although the theoretical volumetric energy density of magnesium–ion batteries is higher than that of lithium–ion batteries, practical studies have revealed that their actual energy density is significantly lower. This is mainly due to the sluggish diffusion kinetics of Mg^{2+} in electrode materials, which prevents sufficient intercalation and deintercalation of magnesium ions[3].

In the early research on cathode materials for magnesium–ion batteries, Chevrel–phase compounds were a typical system that attracted considerable attention. However, Aurbach et al. found that the use of Chevrel–phase compounds as cathodes for magnesium–ion batteries resulted in relatively low energy density[8]. In addition, many researchers have applied transition metal sulfides and oxides (such as MoO_3, MoS_2, TiS_2, MnO_2, etc.) as cathode materials for magnesium–ion batteries, but their cycling stability was generally poor[9]. In recent years, spinel–type transition metal oxides have been widely used as cathode materials for lithium–ion batteries, among which $LiMn_2O_4$ is the most representative[10–12]. On this basis, researchers have further explored the feasibility of using spinel–structured magnesium manganese oxide $MgMn_2O_4$ as a cathode material for magnesium–ion batteries[13]. Nevertheless, studies have shown that such materials are prone to crystal structure distortion due to the significant Jahn–Teller effect. Meanwhile, manganese in the electrode tends to dissolve into the electrolyte. These two factors together lead to severe capacity fading of spinel manganese–based oxides during cycling[14]. Extensive experimental results confirmed that partial substitution of manganese sites with other metal elements can effectively suppress the Jahn–Teller effect, enhance the structural stability of the material, and thereby significantly improve its electrochemical performance[15,16]. Iron is abundant on Earth and low in cost, making it an ideal candidate for manganese substitution, in particular, $MgFe_2O_4$ has been confirmed to exhibit excellent structural stability, yet its relatively compact three–dimensional ion channels are unfavorable for the transport and storage of metal ions[17]. Therefore, the preparation of $MgFe_xMn_yO_4$ electrode materials by combining the respective advantages of the two materials is expected to effectively improve the magnesium–ion storage properties.

As a critical component of magnesium–ion batteries, the electrolyte plays a vital role in ion

transport, interfacial stability, and overall electrochemical performance of the battery. Zhang et al. conducted systematic studies on aqueous magnesium–ion battery systems[18]. Their results showed that when the concentration of acidic electrolytes such as $MgCl_2$ is excessively high, obvious corrosion and dissolution of electrode materials will occur, thereby leading to significant degradation of the cycle life of the battery. On the other hand, an overly low electrolyte concentration cannot guarantee sufficient Mg^{2+} transport and effective intercalation/deintercalation, making it difficult for the battery to achieve an ideal discharge specific capacity. It is worth noting that the introduction of an appropriate amount of manganese ions into the aqueous electrolyte can effectively suppress the dissolution of manganese from spinel–type manganese–containing electrodes during cycling, stabilize the crystal structure of the material, and thus significantly improve the cycle stability and electrochemical performance of the battery[19]. However, most relevant studies have focused on conventional factors such as electrolyte type, concentration, and pH value. The intrinsic influence mechanism of manganese ion concentration in the electrolyte on the structural evolution, interfacial stability, and long–cycle performance of spinel manganese–containing electrodes still lacks systematic investigation, which has become one of the key issues restricting the further improvement of the performance of aqueous magnesium–ion batteries.

In summary, based on $MgMn_2O_4$ and $MgFe_2O_4$ electrode materials, this work combines their advantages to prepare $MgFe_xMn_yO_4$ electrodes. Coupled with the strategy of regulating manganese ion concentration in the electrolyte, it suppresses electrode manganese dissolution from the electrode, improves the structural stability of the electrode material, and further enhances the electrochemical energy storage performance of aqueous magnesium–ion batteries. Firstly, the binary spinel–structured nanomaterial $MgFe_xMn_yO_4$ was prepared via a sol–gel method. A 0.5 M $MgCl_2$ aqueous solution was used as the electrolyte, and manganese acetate was employed as the manganese source to adjust the manganese concentration by controlling the amount of added manganese acetate. The electrochemical performance was tested using a three–electrode system, and the synergistic influence of iron doping and manganese concentration regulation in the electrolyte on the electrochemical properties of the material was systematically investigated.

The results show that the material exhibits optimal electrochemical performance at a manganese acetate concentration of 2.45 mM: at a current density of 1000 $mA \cdot g^{-1}$, its discharge specific capacity reaches 116.6 $mAh \cdot g^{-1}$, and after 250 charge–discharge cycles, the specific capacity only loses 3.77%, showing excellent cycle stability.

2. Experimental Section

2.1 Reagents and Instruments

The main chemical reagents used in the experiment are as follows: magnesium nitrate hexahydrate ($Mg(NO_3)_2 \cdot 6H_2O$) and magnesium chloride hexahydrate ($MgCl_2 \cdot 6H_2O$) (analytical grade, Sinopharm Chemical Reagent Co., Ltd.); manganese nitrate hexahydrate ($Mn(NO_3)_2 \cdot 6H_2O$) (analytical grade, Shanghai Macklin Biochemical Co., Ltd.); iron(III) nitrate nonahydrate ($Fe(NO_3)_3 \cdot 9H_2O$) (analytical grade, Tianjin Tianli Chemical Reagent Co., Ltd.); ethylene glycol (analytical grade, Tianjin Fuyu Fine Chemical Co., Ltd.); citric acid (analytical grade, Tianjin Tianda Chemical Reagent Factory); polyvinylidene fluoride (analytical grade, SOLVAY, France); N–methylpyrrolidone (analytical grade, Tianjin Guangfu Fine Chemical Research Institute). All the above chemical reagents were obtained through commercial channels and used directly in the experiment without any processing or purification.

2.2 Preparation of Electrode Materials and Test Electrodes

In this work, spinel–structured $MgFe_xMn_yO_4$ was prepared by the sol–gel method. The preparation process is shown in Figure 1. First, appropriate masses of $Mg(NO_3)_2·6H_2O$, $Fe(NO_3)_3·9H_2O$, $Mn(NO_3)_2·6H_2O$, citric acid and ethylene glycol were weighed respectively according to a certain molar ratio, and the weighed reagents were dissolved in deionized water. Then, a magnetic stirrer was used for stirring until all solids were dissolved. Subsequently, the resulting solution was heated to 70 °C and continuously stirred for 12 h to convert the solution into a gel. Thereafter, the obtained gel was placed in a blast drying oven and incubated at 200 °C for 12 h. After cooling to room temperature, it was ground into powder with a mortar. Finally, the powder was placed in a muffle furnace and incubated at 550 °C for 12 h to obtain the spinel–structured $MgFe_xMn_yO_4$ nanomaterials.

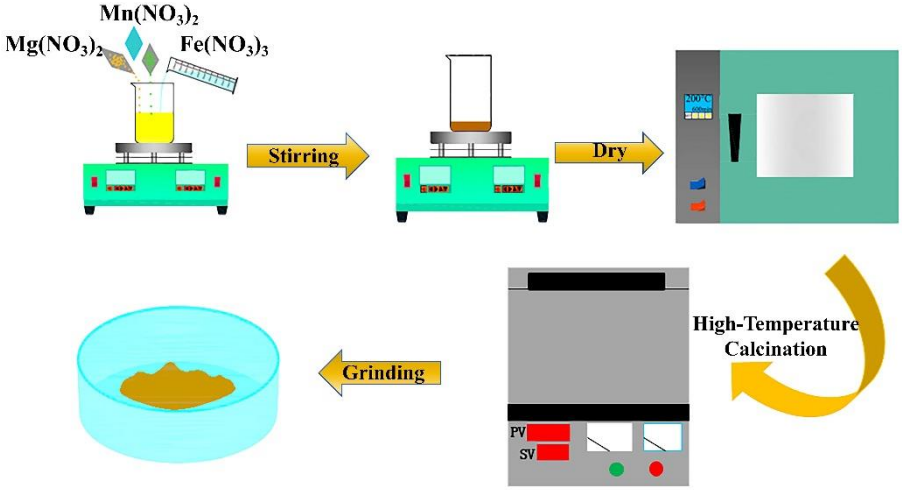

Fig. 1 Preparation flow chart of $MgFe_xMn_yO_4$ electrode material.

The prepared electrode material was mixed uniformly with Super P and PVDF glue at a mass ratio of 8:1:1, and then uniformly coated on the carbon cloth. Finally, the carbon cloth coated with the electrode material was incubated in a vacuum oven at 80 °C for 24 h to obtain the required test electrodes.

2.3 Characterization and Testing

In the experiment, the following instruments were mainly used for structural characterization and performance testing of the electrode materials. X–ray diffraction (XRD, Empyrean, Netherlands) with Cu–Kα radiation was operated at 40 kV and 40 mA, and phase analysis was performed in θ–2θ scan mode with a 2θ range of 10°–90°; Scanning electron microscope (SEM, S–3400N, Hitachi, Japan); X–ray energy dispersive spectrometer (Bruker Corporation, Germany); BET specific surface area analyzer (Model F–Sorb2004, Gold APP Instrument Co., Ltd., Beijing, China); Electrochemical workstation (CHI660E, Chenhua Instrument Co., Ltd., Shanghai, China); Battery test system (LANHE–CT2001A, LAND Electronic Co., Ltd., Wuhan, China).

A three–electrode system was adopted for electrochemical performance testing in this experiment. Specifically, the prepared $MgFe_xMn_yO_4$ material was used as the working electrode, a calomel electrode as the reference electrode, and a carbon rod as the counter electrode. 0.5 M $MgCl_2$ aqueous solutions with different contents of manganese acetate were used as electrolytes. Specifically, 0 g, 0.3 g, 0.4 g and 0.5 g of manganese acetate were added to 500 mL of 0.5 M $MgCl_2$ aqueous solution, corresponding to the molar contents of manganese element of 0 mM, 2.45 mM, 3.26 mM and 4.08 mM, respectively. The above four electrolytes were labeled as M, MM–1, MM–2 and MM–3 in turn.

Cyclic voltammetry tests were performed on a Chenhua CHI660E electrochemical workstation. Galvanostatic charge–discharge cycles and rate performance tests were carried out using a LANHE–CT2001A battery test system.

3. Results and Discussion

First, X–ray diffraction (XRD) and scanning electron microscopy (SEM) were used to characterize the phase structure and morphology of the electrode materials, and the results are shown in Figure 2. It can be seen from the XRD pattern of the electrode material in Figure 2(a) that the diffraction peaks of the prepared electrode sample are completely consistent with the standard card JCPDS Card No: 88–1936, without any impurities, and the intensity of each diffraction peak is relatively strong, indicating that the prepared material has complete crystallization, high phase purity and intact crystal structure[20]. Figure 2(b) is the SEM image of the electrode material. It can be seen from the image that the sample has a relatively uniform particle shape with a nanometer–scale size, about 50 nm, and there are pores between the particles.

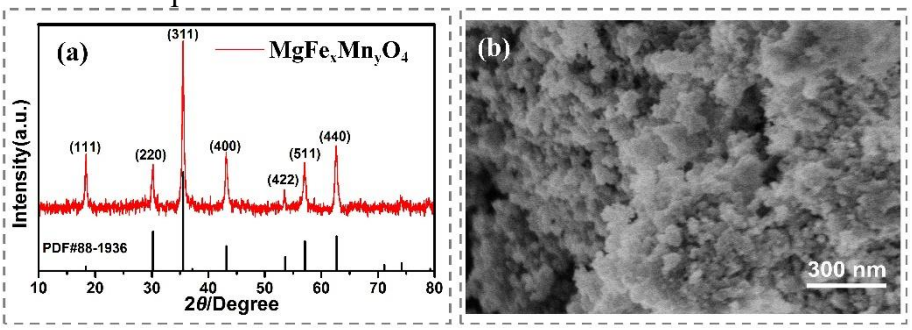

Fig. 2 Structure characterization of the $MgFe_xMn_yO_4$ electrode material. (a) XRD pattern; (b) SEM image.

To further analyze the chemical composition, specific surface area and other characteristics of the material, EDX and BET measurements were performed. As shown in Figure 3(a), the EDX spectrum of the $MgFe_xMn_yO_4$ material confirms the presence of Mg, Mn and Fe elements. The atomic percentages of Fe and Mn are measured to be 20.06% and 8.5%, respectively, and the calculated molar ratio of Fe to Mn is approximately 1.4:0.6, verifying the successful preparation of the $MgFe_xMn_yO_4$ electrode material. Figure 3(b) shows the N_2 adsorption–desorption isotherm of $MgFe_xMn_yO_4$, which can be classified as Type IV, indicating the nanoporous characteristic of the as-prepared electrode material, in good agreement with the BJH pore-size distribution shown in the inset of Figure 3(b)[21]. The specific surface area and average pore diameter are determined to be 46.49 $m^2\ g^{-1}$ and 17.84 nm, respectively.

In previous studies, the voltage window for Mg^{2+} storage in such materials was confirmed to be −0.8 V to 1.1 V. On this basis, galvanostatic charging–discharging tests of the electrode material were first performed using a LANHE battery tester with a three–electrode configuration in four electrolytes: M, MM–1, MM–2, and MM–3. Figures 4(a)–(c) show the first three galvanostatic charge–discharge curves of the active electrode in electrolytes M, MM–1, and MM–2, respectively. The electrode exhibits an initial discharge specific capacity of 127.8 mAh g^{-1} in pure $MgCl_2$ electrolyte (M), while the addition of manganese acetate gives an initial discharge specific capacity of 229.7 mAh g^{-1} in electrolyte MM–2 and only 167.4 mAh g^{-1} in electrolyte MM–3. Figure 5(d) presents the initial charge curve of the active electrode in electrolyte MM–3, in which severe voltage fluctuation occurs during charging as shown in the inset, and the upper charging voltage limit is not reached even after 12 h of charging, resulting in abnormal charge–discharge behavior. This is mainly caused by the formation of abundant deposits on the active electrode surface during cycling, which prevents Mg^{2+}

from inserting into the electrode material (Figure 4(e)), and the measured capacity is thus a false capacity arising from continuous deposition. Figure 5(a) shows the pristine working electrode without any test; Figure 5(b) shows the working electrode after galvanostatic charging–discharging testing in electrolyte M with no deposits observed on the surface; Figures 5(c) and 5(d) show the electrodes after testing in electrolytes MM–1 and MM–2, respectively, with no visible deposits on either surface. By comparison, an obvious deposition layer is formed on the working electrode surface during electrochemical tests when the concentration of manganese acetate in the electrolyte is 4.08 mM (Figure 5(e)).

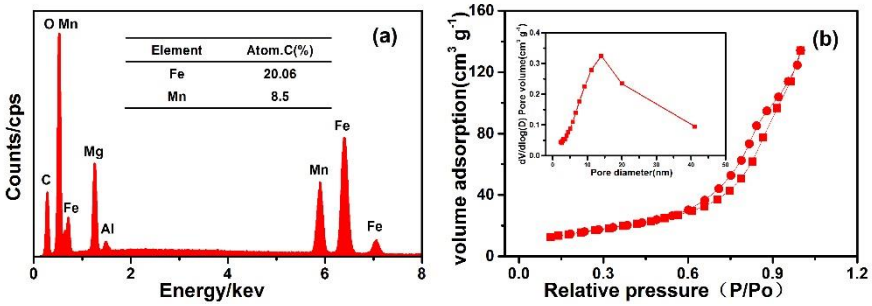

Fig. 3 EDX spectrum of $MgFe_xMn_yO_4$ (a); N_2 absorption and desorption of $MgFe_xMn_yO_4$ (b); The illustration of (b) shows the BJH pore size distribution of $MgFe_xMn_yO_4$.

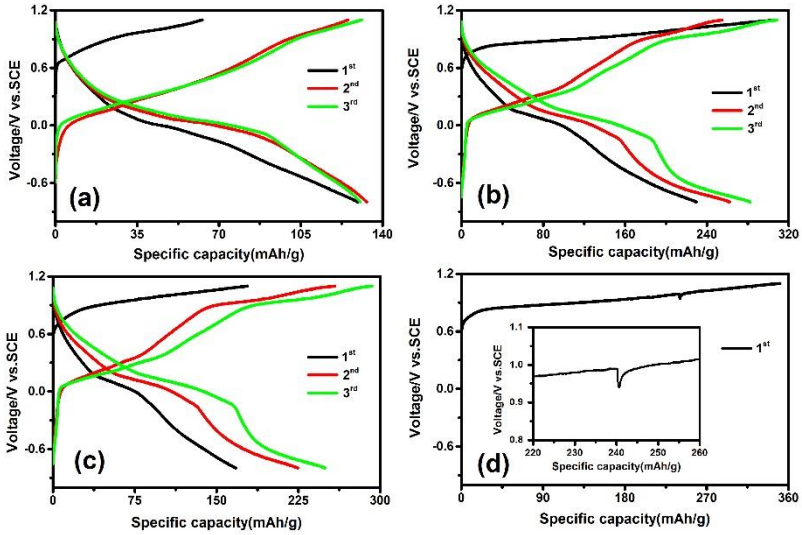

Fig. 4 The first three charge–discharge curves of the $MgFe_xMn_yO_4$ active electrode. (a) Electrolyte M; (b) Electrolyte MM–1; (c) Electrolyte MM–2; (d) Electrolyte MM–3.

Since the prepared electrode was found unable to work normally in MM–3 during the above tests, only three electrolytes, M, MM–1, and MM–2, were used in the subsequent research to further investigate the effect of manganese content in the electrolyte on the electrochemical performance of $MgFe_xMn_yO_4$. Figure 6 shows the cyclic voltammetry curves of the electrode material tested in the above three electrolytes. When the active electrode was tested in electrolyte M, its CV curve exhibited only one pair of distinct redox peaks, as shown in Figure 6(a). In contrast, after adding manganese acetate into the electrolyte, the CV curves exhibited two pairs of distinct redox peaks, as shown in Figures 6(b)–(c). This indicates that the electrochemical reactions of the active material are significantly enhanced during charge–discharge processes in manganese–containing electrolytes, which is beneficial for the electrode material to achieve a higher charge–discharge energy density. Furthermore, at the same scan rate, the peak current measured in electrolyte MM–1 was the largest,

indicating a higher capacity of the electrode material, while the peak current decreased slightly in electrolyte MM–2. For instance, at a scan rate of 5 mV s^{-1}, the peak currents of the active material in electrolytes M, MM–1, and MM–2 were 18.88 mA, 24.44 mA, and 22.18 mA, respectively.

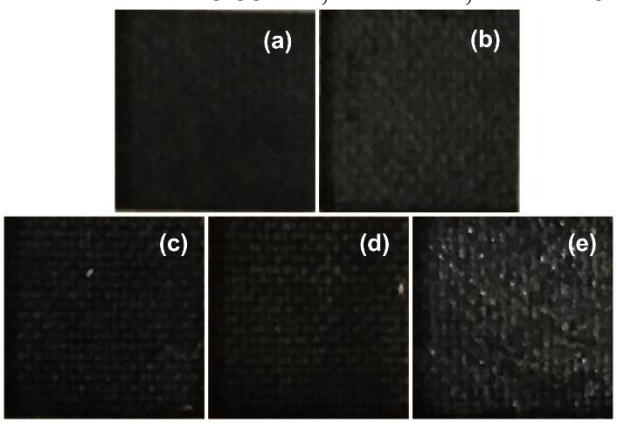

Fig. 5 Photographs of the working electrodes. (a) Working electrode without tested; (b) Working electrodes after tested in electrolyte M; (c) Working electrodes after tested in electrolyte MM–1; (d) Working electrodes after tested in electrolyte MM–2; (e)Working electrodes after tested in electrolyte MM–3.

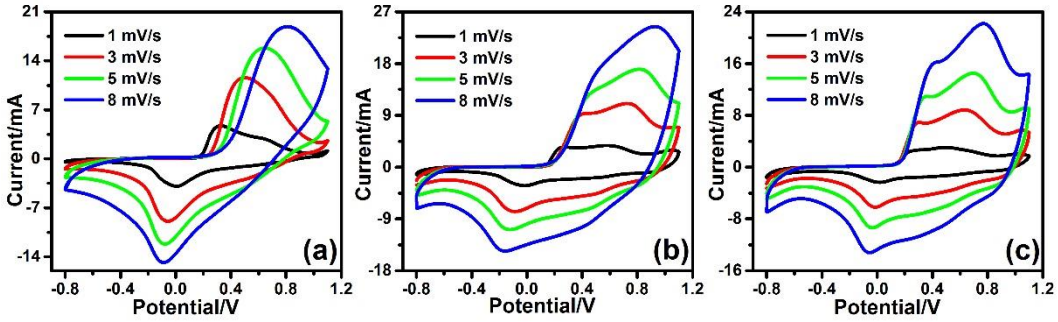

Fig. 6 CV curve of $MgFe_xMn_yO_4$ active electrode. (a) Electrolyte M; (b) Electrolyte MM–1; (c)Electrolyte MM–2.

To illustrate the effect of manganese content in the electrolyte on the Mg^{2+} storage performance of the active material, charge–discharge curves at various current densities were further measured using a LANHE battery tester, with the results shown in Figure 7. Figures 7(a)–(c) display the charge–discharge curves of the electrode material at different current densities (50–1000 mA g^{-1}) in electrolytes M, MM-1, and MM-2, respectively. In electrolyte M, the electrode delivers a discharge specific capacity of 134.6 mAh g^{-1} at 50 mA g^{-1}, which decreases gradually with increasing current density, reaching 74.9 mAh g^{-1} at 1000 mA g^{-1}, corresponding to 55.64% of the capacity at 50 mA g^{-1}. In electrolyte MM-1, the discharge specific capacity reaches 321.5 mAh g^{-1} at 50 mA g^{-1} and remains 116.5 mAh g^{-1} at 1000 mA g^{-1}, nearly 40 mAh g^{-1} higher than that in electrolyte M. In electrolyte MM-2, the discharge specific capacity is 259.1 mAh g^{-1} at 50 mA g^{-1} and 69.7 mAh g^{-1} at 1000 mA g^{-1}, which are 62.4 mAh g^{-1} and 46.8 mAh g^{-1} lower than those in MM-1, respectively. These results confirm that a manganese acetate concentration of 2.45 mM in the electrolyte is optimal, endowing the electrode with the highest discharge specific capacity and best rate capability.

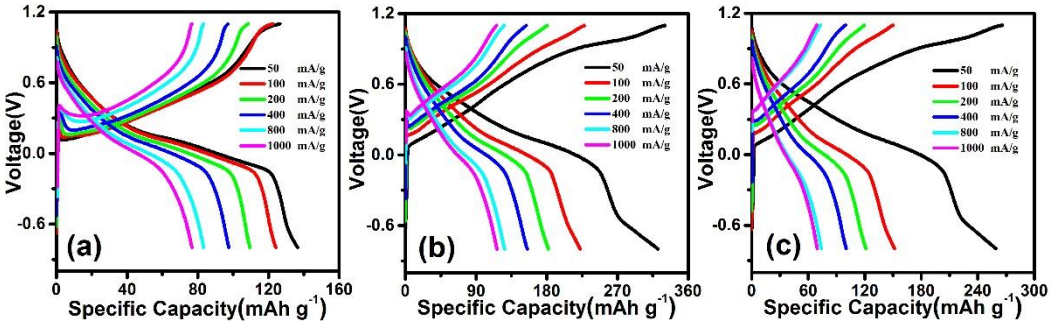

Fig. 7 Charge–discharge curves at different current densities (50–1000 mAh g–1) for electrode materials in three electrolytes. (a) Electrolyte M; (b) Electrolyte MM–1; (c) Electrolyte MM–2.

To further investigate the electrochemical stability of the active electrode in different electrolytes, the rate cycling performance of the $MgFe_xMn_yO_4$ active electrode was tested in three different electrolytes, as shown in Figure 8(a). It can be seen that at relatively low current densities (below 200 mA g^{-1}), the discharge capacity of the electrode material is significantly improved after adding manganese acetate, and the highest discharge specific capacity is achieved in electrolyte MM-1. When tested at current densities above 200 mA g^{-1}, the electrode still delivers the highest discharge specific capacity in electrolyte MM-1, whereas the capacity in electrolyte MM-2 decreases obviously and even becomes lower than that in electrolyte M. These results indicate that the electrode exhibits the best rate cycling performance in 0.5 M $MgCl_2$ aqueous electrolyte with 2.45 mM manganese acetate. Figure 8(b) presents the long-cycle performance of the electrode material at a current density of 1000 mA g^{-1} in different electrolytes. Similar to the rate performance, the electrode achieves the maximum discharge specific capacity of 116.6 mAh g^{-1} in electrolyte MM-1, and remains at 112.2 mAh g^{-1} after 250 cycles, corresponding to a capacity retention rate of 96.23%. Moreover, the coulombic efficiency in this electrolyte is closest to 100%, indicating excellent electrochemical performance. This is mainly attributed to the presence of Mn^{2+} in the electrolyte, which effectively suppresses the dissolution of manganese from the electrode material and thus maintains the structural stability of the material. In contrast, when tested in electrolyte MM-2, the discharge specific capacity decays rapidly and even falls below that in electrolyte M.

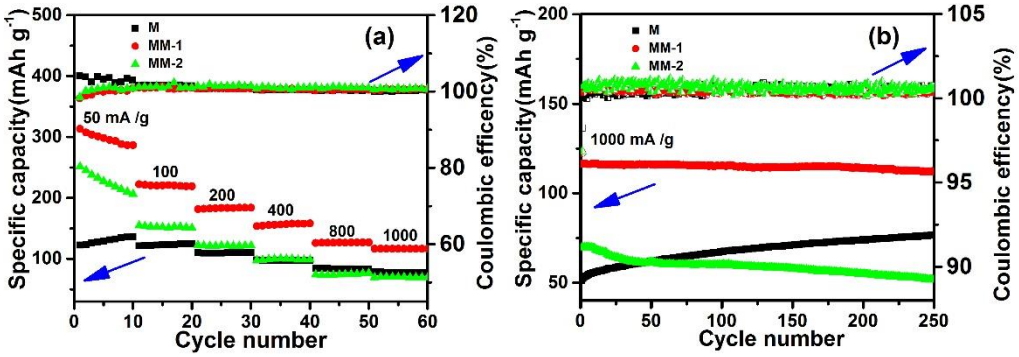

Fig. 8 Magnesium–ion storage performance of the active electrode. (a) Rate performance test chart of electrode materials in three electrolytes; (b) cycle performance test chart in three electrolytes.

4. Conclusion

In this study, spinel–type $MgFe_xMn_yO_4$ nanomaterials were successfully prepared via the sol–gel method. Characterization techniques including N_2 adsorption–desorption, scanning electron microscopy (SEM), and energy–dispersive X–ray spectroscopy (EDX) confirmed that the as–prepared material is a nanocrystalline substance, and also verified the presence of iron and manganese

elements in the electrode material, thus confirming the success of material preparation. By adjusting the concentration of manganese acetate added to the 0.5 M $MgCl_2$ electrolyte, this study systematically investigated the effect of manganese content in the electrolyte on the magnesium–ion storage performance of $MgFe_xMn_yO_4$ electrode materials. The electrochemical test results show that the concentration of manganese acetate in the electrolyte has a significant regulatory effect on the charge–discharge specific capacity, rate capability, and cycling stability of the electrode material: when the concentration of manganese acetate is 2.45 mM (electrolyte MM–1), the electrode material exhibits the optimal electrochemical performance, with a discharge specific capacity of 116.6 mAh g^{-1} at a current density of 1000 mA g^{-1}, and a capacity retention rate of as high as 96.23% after 250 charge–discharge cycles, with a Coulombic efficiency close to 100%. However, an excessively high concentration of manganese acetate (4.08 mM, electrolyte MM–3) leads to the formation of a large amount of deposits on the electrode surface, which hinders the intercalation of magnesium ions and prevents the battery from charging and discharging normally. A too low concentration or no addition of manganese acetate results in low discharge specific capacity and insufficient cycling stability of the electrode material. This study provides experimental basis and theoretical reference for the preparation of high–performance magnesium–ion battery cathode materials and the optimization of electrolyte systems.

Acknowledgements

This work was supported by the Scientific Research Project of Zhejiang Provincial Department of Education (Y202353217 and Y202352960), Scientific Research Foundation of Zhejiang University of Water Resources and Electric Power (xky2023032), The Innovation and Entrepreneurship Training Program for College Students of Zhejiang University of Water Resources and Electric Power (202411481036, 2024; S202411481075, 2024).

References

[1] Saad Mahmud Sonyy, Harun Chowdhury, Firoz Alam and et al. Methodology for estimating and mitigating intermittency in renewable energy sources[J]. Energy Conversion and Management, 2026, 350: 120943.
[2] Akhila Das, Neethu T.M. Balakrishnan, Pranav Sreeram and et al. Prospects for magnesium ion batteries: A compreshensive materials review[J]. Coordination Chemistry Reviews, 2024, 502: 215593.
[3] Quanqing Zhang, Lijie He, Anduo Liu and et al. High–performance Mg–ion battery materials: Recent progress and future perspectives[J]. Journal of Energy Storage, 2025, 132: 117900.
[4] Runjing Xu, Xin Gao, Ya Chen and et al. Research status and prospect of rechargeable magnesium ion batteries cathode materials[J]. Chinese Chemical Letters, 2024, 35: 109852.
[5] Caiyun Sun, Guangsheng Huang, Chaohe Xu and et al. Improved compatibility of aqueous electrolyte with TiO_2(B) toward high–voltage aqueous rechargeable Mg–ion batteries[J]. Energy Storage Materials, 2024, 66: 103197.
[6] Xue Bai, Dianxue Cao, Zhuwu Jiang and et al. Exploration of hydrated lithium manganese oxide with a nanoribbon structure as cathodes in aqueous lithium ion and magnesium ion batteries[J]. Inorganic Chemistry Frontiers, 2022, 9: 485–493.
[7] Ming Liu, Haolin Li, Hongjiang Chi and et al. A review on lithium extraction by electrochemical electrode deionization technology[J]. Journal of Solid State Electrochemistry, 2025, 29: 1577–1592.
[8] D. Aurbach, Z. Lu, A. Schechter and et al. Prototype systems for rechargeable magnesium batteries[J]. Nature, 2000, 407(6805), 724–727.
[9] Minglei Mao, Tao Gao, Singyuk Houa and et al. A critical review of cathodes for rechargeable Mg batteries[J]. Chemical Society Reviews, 2018, 47: 8804.
[10] Bharti Rani, Jitendra Kumar Yadav, Priyanka Saini and et al. $LiMn_2O_4$ as a cathode material: challenges and opportunities for lithium–ion batteries[J]. Sustainable Energy & Fuels, 2025, 9: 4262–4285.
[11] R. Trócoli, A. Morata, C Erinmwingbovo and et al. Self–discharge in Li–ion aqueous batteries: A case study on $LiMn_2O_4$[J]. Electrochimica Acta, 2021, 373: 137847.
[12] O M Sousa, L V C Assali, M V Lalic and et al. Charging behavior of $ZnMn_2O_4$ and $LiMn_2O_4$ in a zinc– and lithium–ion battery: an ab initio study[J]. Journal of Physics: Energy, 2024, 6: 025025.

[13] Naomi Nishimura, Kazumasa Masaki, Wei Tan and et al. Spray–Dried $MgMn_2O_4$ Spinel Oxide Cathode with Single Mg Ion–Conductive Polymers for Rechargeable Mg Metal Battery[J]. The Journal of Physical Chemistry C, 2023, 127: 11829–11835.
[14] Huilin Pan, Yuyan Shao, Pengfei Yan and et al. Reversible aqueous zinc/manganese oxide energy storage from conversion reactions[J]. Nature energy, 2016, 1: 16039.
[15] Rosnadiya Rosli, Othman Othman, Nurhidayu Haji Harudin and et al. Development of al–doped $MgMn_2O_4$–based cathode materials for magnesium ion cells[J]. International Journal of Applied Ceramic Technology. 2023, 20: 2371–2381.
[16] R. Thirunakaran, R. Ravikumar, S. Vanitha and et al. Glutamic acid–assisted sol–gel synthesis of multi–doped spinel lithium manganate as cathode materials for lithium rechargeable batteries[J]. Electrochimica Acta, 2011, 58: 348–358.
[17] Oumayema El Ghali, Zakaria Chchiyai, Said Mansouri and et al. Enhanced electrochemical performance of $MgFeO_4$ spinel as anode materials for Lithium–ion batteries through manganese doping[J]. Materials Today Communications, 2024, 40: 109532.
[18] Hongyu Zhang, Ke Ye, Shuangxi Shao and et al. Octahedral magnesium manganese oxide molecular sieves as the cathode material of aqueous rechargeable magnesium–ion battery[J]. Electrochimica Acta, 2017, 229: 371–379
[19] Ning Zhang, Fangyi Cheng, Junxiang Liu and et al. Rechargeable aqueous zinc–manganese dioxide batteries with high energy and power densities[J]. Nature Communications, 2017, 8: 405.
[20] Chengsi Pan, Ralph G. Nuzzo and Andrew A. Gewirth. $ZnAl_xCo_{2-x}O_4$ Spinels as Cathode Materials for Non–Aqueous Zn Batteries with an Open Circuit Voltage of ≤2 V[J]. Chemistry of Materials, 2017, 29: 9351–9359.
[21] Rosendo López, Ricardo Gómez and María Elena Llanos. Photophysical and photocatalytic properties of nanosized copper–doped titania sol–gel catalysts[J]. Catalysis Today, 2009, 148: 103–108.